



## Multi-hazard stress testing under extreme rainstorms in the Shenzhen metropolitan area

Yejia Qiang<sup>a,b</sup>, Te Xiao<sup>ID C</sup>, Jian He<sup>a</sup> and Limin Zhang<sup>a,d</sup>

<sup>a</sup>Department of Civil and Environmental Engineering, The Hong Kong University of Science and Technology, Hong Kong, People's Republic of China; <sup>b</sup>Guangdong Provincial Academy of Building Research Group Co., Ltd., Guangzhou, People's Republic of China; <sup>c</sup>State Key Laboratory of Ocean Engineering, Shanghai Key Laboratory for Digital Maintenance of Buildings and Infrastructure, Department of Civil Engineering, Shanghai Jiao Tong University, Shanghai, People's Republic of China; <sup>d</sup>HKUST Shenzhen-Hong Kong Collaborative Innovation Research Institute, Shenzhen, People's Republic of China

### ABSTRACT

A severe rainstorm can trigger numerous natural hazards of multiple types in cities with hilly terrain, such as landslides, debris flows, and flooding. Such compound hazards may pose much greater risks than a single hazard to the safety of residents and infrastructures. This study focuses on a metropolitan area of Shenzhen, China and develops a multi-hazard stress testing method for hazard risk management against extreme rainstorms. The probable maximum precipitation in Shenzhen is first estimated using the storm transposition method considering orographic intensification and moisture maximisation, with the centre peak amount being 1441 mm in 24 hours at Tanglang Mountain. An integrated physically-based multi-hazard simulation model, EDDA, is then utilised to simulate the processes of initiation, propagation and transformation of landslides, debris flows and flooding in a unified manner. Under the designated extreme rainstorms of a 1000-year return period and 85% of probable maximum precipitation, deposit depths of landslides and debris flows can be large in some urban areas near the foot of Tanglang Mountain; flooding can be very extensive in the flat built-up regions, with 21.8% and 31.7% of the study area flooded, respectively. The produced multi-hazard maps can facilitate the design of risk mitigation measures against extreme rainstorms.

### ARTICLE HISTORY

Received 22 July 2024  
Accepted 12 December 2024

### KEYWORDS

Probable maximum precipitation; multi-hazard analysis; stress testing; landslides; debris flows; flooding

## 1. Introduction

Extreme rainstorms will be more frequent and intense in the future due to climate change (IPCC 2012; Qiang, Zhang, and Xiao 2020), which may trigger many types of natural hazards. In low-land urban areas, intensive rainstorms may lead to sewer surcharge, water logging, and river flooding (Qiang et al. 2021a; Du et al. 2024; Gao et al. 2019, 2023a, b; He et al. 2023; Ramakrishnan et al. 2022). In mountainous areas, rainstorms can induce excess runoff on the surface of hillslopes and raise the groundwater table inside hillslopes, which may cause surface erosion, landslides, and debris flows (Guo et al. 2023; Han et al. 2024; Lu et al. 2024; Tien Bui et al. 2017; Xiao et al. 2023; Xiao and Zhang 2023; Zhang et al. 2011). These hazards may form catastrophic hazard chains, further amplifying the damage in both time and space domains. For example, an extreme rainstorm with a maximum hourly rainfall amount of 201.9 mm hit Henan Province, China in July 2021, causing severe urban and river flooding, landslides, dam breaching, and extensive inundation

of underground space. About 15 million people were affected and 398 people were dead or missing. In the design of engineering mitigation works against landslides and floods, rainstorms with 10-year or 50-year return periods are often referred to, but more extreme events may not be considered due to cost constraints. Nevertheless, the society still should be prepared to answer questions such as “what hazard scenarios will happen in extreme rainstorms” and “what hazard mitigation measures should be taken” for emergency management and risk adaptation.

In conventional risk assessment, the consequences of extreme events are likely to be ignored due to their low occurrence probabilities. Instead, stress testing can be an alternative to rationally investigate such extreme events (Gao, Zhang, and Chen 2015; He et al. 2021; Zhou, Gao, and Zhang 2019). A risk-informed stress test includes five steps (after Zhang et al. (2017)): (1) quantifying stress scenarios; (2) simulating hazard processes; (3) assessing hazard consequences and risks; (4) identifying weakness and bottlenecks of the current hazard mitigation system and developing improved

hazard mitigation strategies; and (5) evaluating the effectiveness of new strategies in terms of risk reduction. In the abovementioned procedure, the quantification of stress scenarios (i.e. extreme rainstorms) and the analysis of hazard processes as well as consequences are the key tasks and the basis for developing mitigation strategies.

To properly design extreme rainstorms as stress scenarios for hazard analysis, region-specific rainstorm records are the most reliable references and are always applied to identify locations prone to flooding, landslides, and other hidden hazards (Clarke and Rendell 2006; Kumar et al. 2017; Regier, Naughton, and McDonald 2022). The depth-area-duration analysis is widely used to capture the characteristics of extreme storms (Oguz et al. 2024; WMO 1969). In addition, the concept of probable maximum precipitation (PMP) is often used to indicate the physical upper limits of storms for a certain storm area, which is an important reference for evaluating potential risks of storm-related hazards. Many methods have been developed to estimate PMP (WMO 2009), such as the local method, transposition method, combination method, statistical method, and simulation method. The storm transposition method has been used in recent PMP updating studies in Hong Kong (Lin 2015; Lin 2017), in which a severe storm in Taiwan was transposed. The rainstorm of 85% PMP, corresponding to a 10,000-year return period, is often taken as a very extreme scenario for hazard analysis (Ho, Lacasse, and Picarelli 2017; Zhou, Gao, and Zhang 2019).

Regarding multi-hazard analysis, many studies conduct independent analyses of different types of hazards and then superpose all layers of single hazards to identify areas where multiple types of hazards may occur (Dilley et al. 2005; Shi et al. 2015). The total risk is taken as a simple summation or weighted summation of individual hazards (Lyu and Yin 2023; Van Westen, Van Asch, and Soeters 2006). However, in case of sequential or simultaneous occurrence of multiple hazard events, one hazard may trigger or amplify the damage of another hazard unexpectedly (Peng and Zhang 2012, 2013). For example, landslides and debris flows may rush into residential areas and block the urban drainage system, resulting in more extensive inundation areas. Therefore, the interaction mechanisms between individual hazards should be properly considered in multi-hazard analysis (Ba et al. 2021; Cascini et al. 2021; Kappes et al. 2012; Tilloy et al. 2019; Wang, He, and Weng 2020), which is possible through physically based models. Destro et al. (2018) proposed a coupled framework for flash flood and debris flow modelling. Bout et al. (2018) developed a multi-hazard

analysis model integrating flash floods, debris flows, and shallow slope failures. Fan et al. (2020) simulated the multi-hazard chain scenarios through the integration of four numerical models for landslide initiation, debris movement, dam breaching, and flood routing, respectively. Since flooding, landslides and debris flows are usually described by different physical equations, the hazard interactions involved need to be manually identified. Such a manner is not feasible when numerous hazard events occur simultaneously in an extreme rainstorm.

The primary objective of this paper is to investigate the compound effects of multiple hazards, including landslides, debris flows, and flooding, in hilly urban regions under possible extreme rainstorms. Several rainstorm scenarios are designed for stress testing, including historical major rainstorms and extreme events quantified by return periods and PMP. An in-house integrated numerical model, EDDA, is applied to simulate the processes of initiation, propagation and transformation of the three types of hazards in a unified manner. The central metropolitan region of Shenzhen, China is taken as a case study. The simulated hazard maps can be used to identify hazard-prone areas and to design hazard mitigation measures against extreme rainstorms.

## 2. Multi-hazard modelling under extreme rainstorms

### 2.1. Interactions among rain-induced hazards

Multiple natural hazards can be induced by intense rainfall, among which landslides, debris flows, and flooding are major types (Figure 1). In areas with steep terrain, slope failures occur due to the rise of groundwater table caused by the infiltration of stormwater. Some of the detached materials, together with the excess surface runoff, may transform into debris flows or debris floods. The bed soils may be eroded by surface runoff and hillslope debris flows may thus initiate. The magnitude and morphology of debris can vary during the process of propagation due to the entrainment of materials from additional slope failures and bed erosion (Shen et al. 2018). The landslide debris would travel a long distance along the channel and may deposit in urbanised areas near hillsides. The blockage of urban drainage system or river network would induce widespread inundation. In the meantime, flooding caused by intense rainfall is another major hazard in relatively flat regions. The inundation may erode surface soils and trigger more failures of man-made slopes in urban settings. Considering the complex interactions among landslides, debris flows, and flooding, an

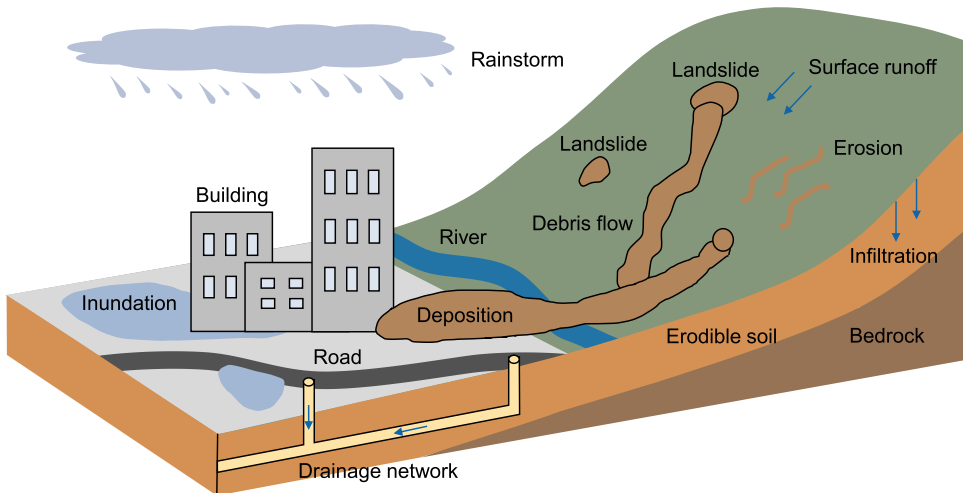


**Figure 1.** Formation of multiple hazards in urban settings under a large rainstorm (modified from Shen et al. (2018)).

integrated numerical model is required to simulate the initiation, propagation, and transformation of multi-hazard processes in a unified manner.

## 2.2. Integrated multi-hazard modelling

In this study, a cell-based integrated numerical model, EDDA (Chen and Zhang 2015; Shen et al. 2018), is adopted to simulate the whole processes of multi-hazard initiation, motion, entrainment, deposition, and property changes. When rain starts, infiltration analysis is first carried out for an infinite two-layer soil slope system in each cell by solving the 1-D Richards equation. The factor of safety of each cell is then evaluated using a 1-D infinite slope stability model based on the pore water pressure profile obtained.

Once a slope fails, the landslide materials will be lumped with surface runoff and surface erosion, forming a flow mixture. The overland flow dynamics can be described by depth-integrated equations of mass conservation and momentum conservation (Chen and Zhang 2015; Shen et al. 2018):

$$\frac{\partial h}{\partial t} + \frac{\partial(hv)}{\partial x} = iC'_{v*} + AC'_{vA} \quad (1)$$

$$\frac{\partial(C_v h)}{\partial t} + \frac{\partial(C_v hv)}{\partial x} = iC_{v*} + AC_{vA} \quad (2)$$

$$\begin{aligned} \frac{\partial v}{\partial t} + v \frac{\partial v}{\partial x} &= -g \left[ \operatorname{sgn}(v) S_f + \frac{\partial(z_b + h)}{\partial x} \right] \\ &- \frac{v}{h} (iC'_{v*} + AC'_{vA}) \end{aligned} \quad (3)$$

where  $x$  is the distance along the flow direction;  $t$  is the time;  $h$  is the flow depth;  $v$  is the depth-averaged flow velocity;  $i$  is the erosion rate ( $>0$ ) or deposition rate ( $<0$ );  $A$  is the rate of material entrainment from

detached landslide materials;  $C_v$  is the volumetric sediment concentration of the flow mixture;  $C_{v*}$  and  $C_{vA}$  are the volume fraction of solids in the erodible bed and entrained surficial materials, respectively;  $C'_{v*} = C_{v*} + (1-C_{v*})s_b$  and  $C'_{vA} = C_{vA} + (1-C_{vA})s_A$ , in which  $s_b$  and  $s_A$  are the degrees of saturation in the erodible bed and entrained surficial materials, respectively;  $g$  is the gravitational acceleration;  $S_f$  is the energy slope;  $z_b$  is the bed elevation; and  $\operatorname{sgn}(\cdot)$  is the signum function that is used to ensure the direction of the flow resistance is opposite to that of the flow direction.

For practical implementation, the slope stability during the whole rainstorm process is first evaluated to identify the location, time and depth of slope failures. The flow process is then simulated, with the types of flow mixture distinguished with the volumetric solid concentration  $C_v$ . According to FLO-2D (2018), the flow mixture can be classified into four types: clear water flow ( $C_v < 0.2$ ), debris flood ( $0.2 < C_v < 0.45$ ), debris flow ( $0.45 < C_v < 0.6$ ), and landslide ( $C_v > 0.6$ ). In this study, debris flood and debris flow are lumped together as debris flow for simplicity, i.e. a mixture with  $C_v$  between 0.2–0.6. Different rheological models are used to describe the energy slopes  $S_f$  for different types of flow mixtures. For clear water flow ( $C_v < 0.2$ ),  $S_f$  is determined based on Manning's equation; for other flows with  $C_v > 0.2$ ,  $S_f$  is quantified by a quadratic rheological model (O'Brien, Julien, and Fullerton 1993; Shen et al. 2018), which combines yield slope, viscous slope, and turbulent-dispersive slope, and varies as  $C_v$  changes. By this means, EDDA can simulate landslides, debris flows, and flooding in a unified framework. The complex hazard interactions have been modelled inherently through the solid material exchange (i.e. erosion and deposition) between the flow mixture and soil bed. In

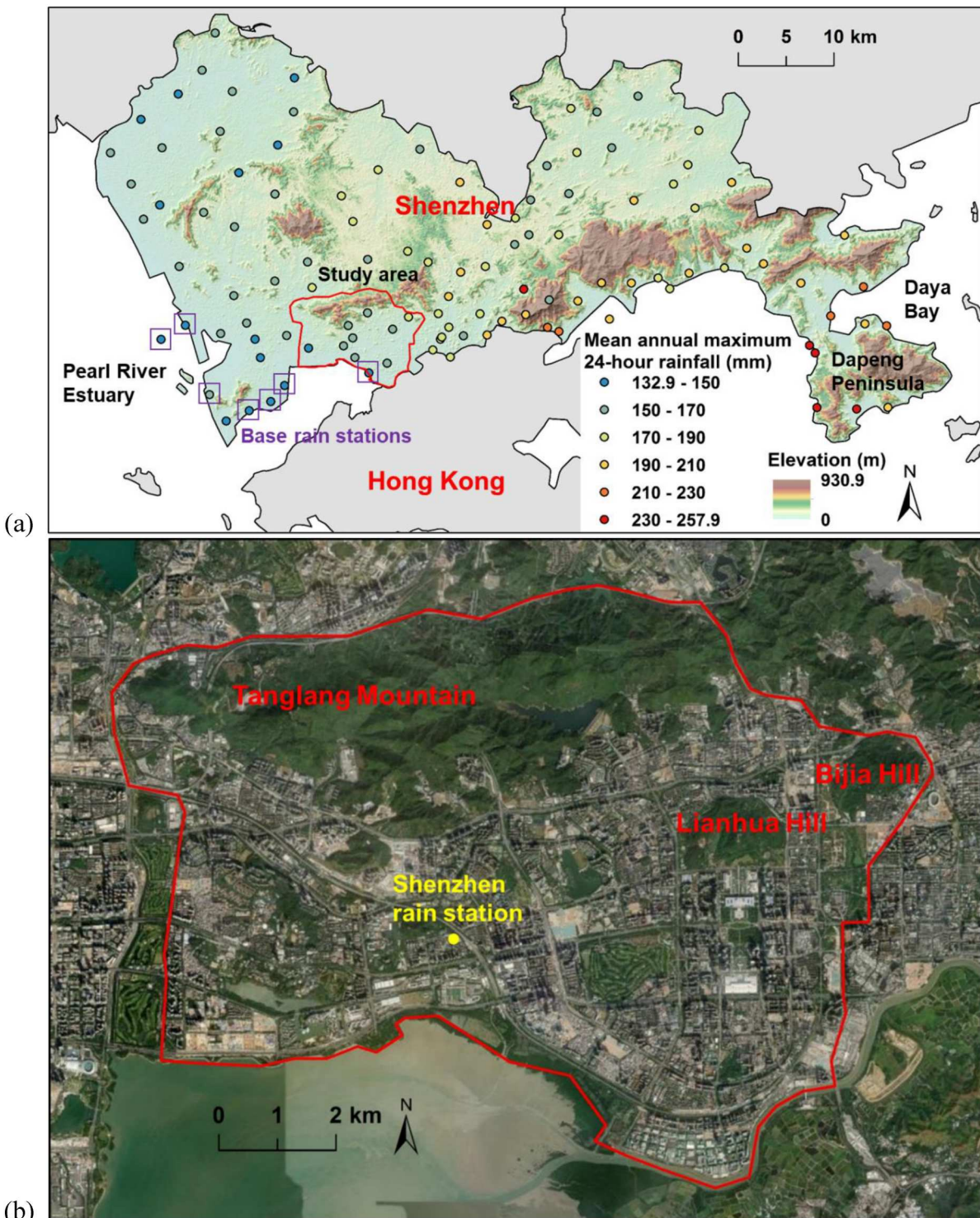


Figure 2. Study area: (a) Shenzhen; (b) selected metropolitan area.

EDDA, erosion occurs when bed shear stress is larger than the critical erosive shear stress of the bed and  $C_v$  is smaller than an equilibrium value, while deposition occurs when the flow velocity is smaller than a critical value and  $C_v$  is larger than an equilibrium value. Changes in flow depth and  $C_v$  within each cell are evaluated at every time step considering surface

runoff, slope failure mass entrainment, erosion, and deposition.

In densely populated urban regions, influences of building blockage on the flow are considered by an area reduction factor (i.e. reduction in water storage) and eight width reduction factors for different flow directions (i.e. reduction in flow width for a certain direction),

**Table 1.** Severe rainstorms in the recent history of Shenzhen.

No	Date	Storm type	Storm centre	Maximum rainfall (mm) [recorded rain station]			Consequences
				1-hour	3-hour	6-hour	
1	13–14 June 2008	Trough	Bao'an District, Guangming District	110.3 [Heping Community]	–	–	Over 100 slope failures; over 500 flooding spots; over 70 house collapses; over one million residents affected; 8 people died or missing; direct economic loss of CNY 490 million
2	11 May 2014	Front	Longhua District	89.3* [Longhua]	211.5* [Longhua]	319.8 [Longhua]	370.4* [daily; Shiyuan Reservoir]
3	17 May 2014	Front	Pingshan District	119.9 [Tiantou]	235.9 [Tiantou]	267.8* [Tiantou]	458.2* [Longhua]
4	20–21 May 2016	Trough	Dapeng District	107.6* [Nan'ao]	224.5 [Nan'ao]	344.8 [Nan'ao]	344.7* [Tiantou]
5	6–8 June 2018	Typhoon	Yantian District	124.8 [Yantian Port]	184.7* [Sanzhoutian]	256.1* [East OCT]	463 [Youganwan]
6	29–31 Aug. 2018	Trough	Luohu District; Pingshan District	112.4	165.8* [Shanglilang]	227.2* [Sanlian]	About 226 flooding spots; the deepest inundation depth reached 1.5 m
7	7–8 Sep. 2023	Typhoon & Monsoon	Luohu District	116.8 [Luohu]	246.8 [Yantian]	355.2 [Luohu]	Over 260 flooding spots; over 200 people trapped

Note: \*Calculated from rain gauge data.

according to O'Brien, Julien, and Fullerton (1993). They are determined for each cell based on the ratio of occupied area of buildings over the entire area or along one flow direction. If the information on the urban drainage network is available, the drainage flow can be modelled as pipe flow using 1-D Saint-Venant equations (Zhou 2020); otherwise, the capacity of the urban drainage network can be considered using an equivalent drainage method (Qiang et al. 2021b). The equivalent drainage method approximates the drainage capacity of an urban drainage system with enhanced infiltration, in which an infiltration adjustment factor  $K$  is adopted to quantify the permeability ratio of the urban artificial surface over vegetated land. The factor can be calibrated using a physically based drainage model for an area with a similar drainage design standard (Qiang et al. 2021b).

### 2.3. Extreme storm design using storm transposition method

To design extreme rainstorms for stress testing, the storm transposition method is adopted in this study to estimate the PMP. The method assumes that storms observed in history are equally likely to happen in meteorologically and topographically homogeneous regions. To make the storm transposition possible among meteorologically homogeneous regions, the impact of topographic difference between the target area (where the storm happened) and the design area (where the storm will be transposed to) needs to be considered. A storm separation technique called the step duration orographic intensification factor method (Lin 2015) can be used to separate rainfall into components caused by atmospheric forcing (non-orographic) and caused by terrain forcing (orographic), which allows the convergence component (i.e. non-orographic component) to be transposed to a wider area. The averaged orographic intensification factor OIF over a time interval ( $T$ ) for a given location ( $x$ ) is defined as (Lin 2015):

$$\text{OIF}_T(x) = \frac{R_T(x)}{R_{0,T}(x)} \quad (4)$$

where  $R_T(x)$  is the total rainfall amount containing the orographic influence; and  $R_{0,T}(x)$  is the rainfall amount without the orographic influence during  $T$  for the same location. In this study, a 24-hour rainfall interval is considered for estimating the 24-hour PMP.

Since the rainfall recorded on flatlands and in coastal areas in the storm moisture inflow jet route is often regarded as not influenced by the topography, the rain stations located in these areas can be chosen as base stations to estimate the value of  $R_{0,T}(x)$ . To reduce the

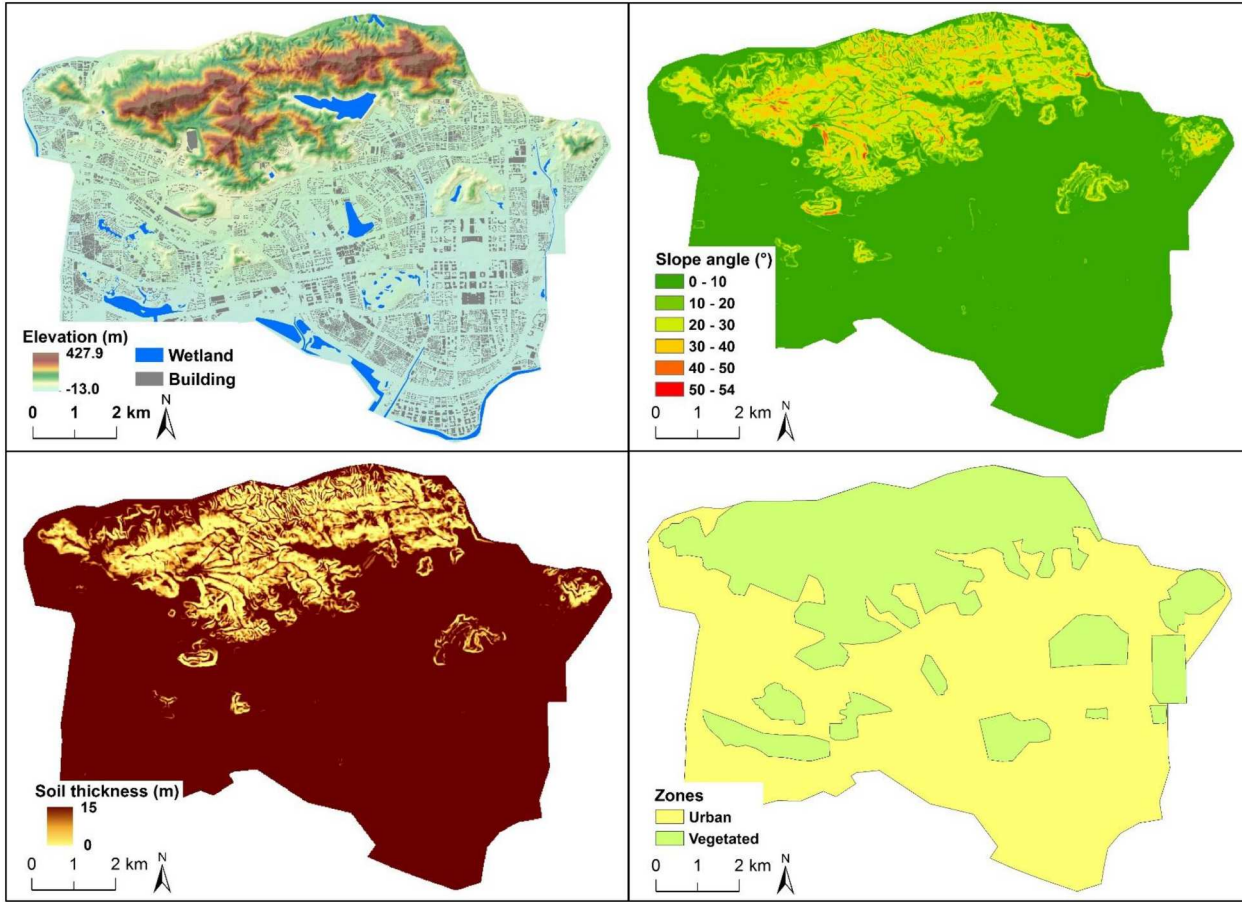


**Figure 3.** Basic data layers for multi-hazard analysis.

sampling error, the average of the means of 24-hour annual maximum rainfall over all base stations is taken. For a specific rain station, the mean of 24-hour annual maximum rainfall is taken as  $R_T(x)$  to calculate  $OIF_T(x)$  at this location. With the orographic intensification factor pattern in the target area, the convergence component of historical severe storms can be derived and then transposed to the design area, and a PMP embryo (i.e. preliminary PMP estimate) can be generated from the transposed convergence component (given a certain orientation) coupled with a local

orographic intensification factor pattern in the design area.

The embryonic PMP should be further adjusted to consider the moisture maximisation. The moisture maximisation ratio  $r_m$ , defined as the storm rainfall amount adjusted in the design area over the transposed storm rainfall amount in the target area, can be determined as the ratio of precipitable water (Lin 2015):

$$r_m = \frac{W_M}{W_S} \quad (5)$$

**Table 2.** Model parameters used in EDDA.

Parameters	Vegetated land	Urban hard surface	References
Effective cohesion, $c$ (kPa)	4	–	Zhou, Gao, and Zhang (2019)
Internal friction angle, $\varphi_b$ (°)	37	–	Zhou, Gao, and Zhang (2019)
Density, $\rho_s$ (kg/m <sup>3</sup> )	2650	–	Zhou, Gao, and Zhang (2019)
Permeability, $k_s$ (m/s)	$4.44 \times 10^{-6}$	$4.44 \times 10^{-6} \times K$	FLO-2D (2018), Qiang et al. (2021a)
Saturated volumetric water content, $\theta_s$	0.5	0.2	Zhou, Gao, and Zhang (2019)
Residual water content, $\theta_r$	0.27	0.07	Zhou, Gao, and Zhang (2019)
Material parameter, $a$	0.7	0.7	Zhou, Gao, and Zhang (2019)
Volume fraction of solids in erodible bed, $C_v^*$	0.65	–	Chen and Zhang (2015)
Degree of saturation of erodible bed, $s_b$	1	–	Chen and Zhang (2015)
Manning's coefficient, $n$	0.15	0.05	FLO-2D (2018)
Resistance parameter for laminar flow, $K_r$	2500	2500	FLO-2D (2018)
Coefficient of deposition rate, $\delta_d$	0.02	0.03	Chen and Zhang (2015)

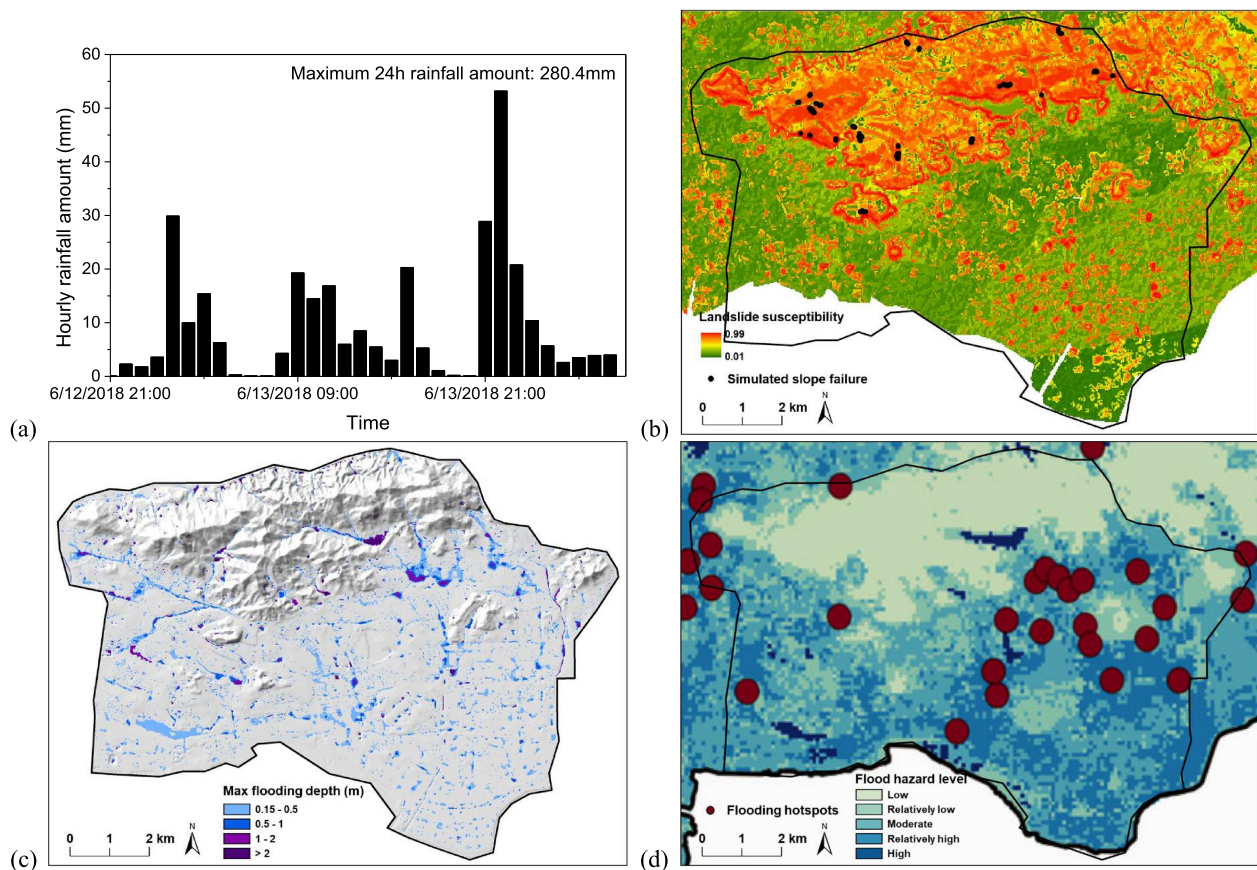


**Figure 4.** Validation of the 2008 rainstorm: (a) rainfall process; (b) simulated landslides vs. landslide susceptibility map (Xing et al. (2021)); (c) simulated flooding spots; (d) flood hazard map (Sarica et al. (2021)).

where  $W_M$  is the maximum precipitable water for the historical maximum dew point in the design area; and  $W_S$  is the precipitable water for the representative storm dew point in the target area. Eventually, the possible PMP estimates can be obtained by multiplying the embryonic PMP by  $r_m$ .

### 3. Case study of the Shenzhen metropolitan area

#### 3.1. Study area

Shenzhen is one of the central cities in the Guangdong-Hong Kong-Macao Greater Bay Area and is the first special economic zone of China. It is located on the east of the Pearl River Estuary and connected to Hong Kong by the Shenzhen River in the south (Figure 2(a)). The total area of the mega city is 1997.47 km<sup>2</sup>, with a population of 17.79 million as of 2023. The average annual rainfall amount (1952–2019) of the city is 1910mm, 86% of which is concentrated in the rainy season from April–September. Affected by the coastal and mountainous terrain, as well as frontal rain and typhoon rain in summer, Shenzhen suffers from frequent

flooding and landslide-related geohazards. Table 1 summarises seven severe storms in the recent history of Shenzhen based on the annual Shenzhen Climate Bulletin from 2007–2023 and available rain gauge data. The severe rainstorm on 13–14 June 2008 which resulted in over 100 landslides and 500 flooding spots, affecting over one million people and causing 8 fatalities, will be used to validate the hazard analysis model.

The study area (Figure 2(b)) is a central metropolitan region of Shenzhen, including part of Futian District and part of Nanshan District, with a total area of 94.6 km<sup>2</sup>. Tanglang Mountain (432 m) is the highest peak in the study area, where landslides and debris flows are likely to happen during intense rainstorms. The southern part of the study area is relatively flat and prone to flood hazards.

#### 3.2. Model development and validation

A multi-hazard analysis model is developed for the study area using EDDA. The grid size is 20 m and the total number of cells is 236,510. Parameters for each cell include elevation, slope gradient, soil thickness, land use, material properties, etc., as shown in Figure 3

**Table 3.** Mean annual maximum 24-hour rainfall amounts and orographic intensification factors at rain stations in Shenzhen.

No.	Station ID	Lon (°E)	Lat (°N)	Elevation (m)	Mean annual maximum 24-hour rainfall amount (mm)	OIF
1	G1120	114.13	22.55	113.0	159.94	1.09
2	G1121	114.11	22.56	17.0	188.01	1.29
3	G1125	114.32	22.61	40.1	187.11	1.28
4	G1129	114.11	22.53	51.0	171.08	1.17
5	G1130	114.05	22.53	120.0	158.14	1.08
6	G1135	114.05	22.56	28.0	156.13	1.07
7	G1142*	113.91	22.48	36.0	149.65	1.02
8	G1151	113.82	22.67	23.8	146.06	1.00
9	G1155	114.01	22.66	76.0	177.33	1.21
10	G1162	114.47	22.60	64.0	198.18	1.36
11	G1163	114.42	22.63	29.0	192.81	1.32
12	G1166	114.12	22.61	90.0	196.59	1.34
13	G1173	114.17	22.56	47.0	195.38	1.34
14	G1174	114.19	22.59	56.0	230.15	1.57
15	G3501	114.00	22.54	56.0	152.73	1.04
16	G3502	113.89	22.65	50.1	156.76	1.07
17	G3521	113.89	22.47	104.1	150.00	1.03
18	G3522	114.10	22.55	18.5	182.10	1.25
19	G3523	114.10	22.55	110.5	170.39	1.17
20	G3524	114.15	22.55	75.1	192.36	1.32
21	G3525	114.50	22.57	25.8	214.40	1.47
22	G3526	113.77	22.72	1.7	169.69	1.16
23	G3527	114.10	22.57	117.7	183.75	1.26
24	G3528	113.95	22.76	39.2	151.60	1.04
25	G3529	113.89	22.78	32.8	163.89	1.12
26	G3530	113.91	22.56	40.7	167.06	1.14
27	G3531	113.90	22.70	57.9	143.51	0.98
28	G3532	113.87	22.84	39.9	167.65	1.15
29	G3533	114.53	22.60	52.0	225.96	1.55
30	G3534	114.14	22.57	42.0	174.11	1.19
31	G3535	114.22	22.56	38.5	213.83	1.46
32	G3536	114.34	22.60	51.7	176.46	1.21
33	G3537	114.37	22.75	46.6	181.39	1.24
34	G3538	114.34	22.69	83.8	180.18	1.23
35	G3539	114.30	22.78	55.0	159.66	1.09
36	G3540*	113.93	22.49	19.3	148.19	1.01
37	G3541	114.51	22.65	40.0	195.91	1.34
38	G3543	114.04	22.71	65.8	170.25	1.16
39	G3544	114.39	22.62	15.4	187.74	1.28
40	G3546	113.91	22.55	51.0	147.39	1.01
41	G3548	113.93	22.60	40.0	161.60	1.10
42	G3549	114.27	22.60	362.6	191.55	1.31
43	G3550	113.84	22.78	59.3	143.31	0.98
44	G3551	114.00	22.68	81.5	170.03	1.16
45	G3553	114.03	22.62	92.5	169.55	1.16
46	G3554	114.22	22.65	78.6	182.93	1.25
47	G3555	113.92	22.53	104.4	148.15	1.01
48	G3556*	113.87	22.50	25.0	153.21	1.05
49	G3557	113.82	22.73	22.6	159.36	1.09
50	G3558	114.15	22.62	62.9	184.94	1.26
51	G3559	114.12	22.70	84.1	197.10	1.35
52	G3560	114.19	22.65	86.8	164.91	1.13
53	G3561	113.97	22.54	33.0	149.06	1.02
54	G3562	114.03	22.57	63.5	156.59	1.07
55	G3563	114.48	22.54	45.9	244.55	1.67
56	G3564	114.24	22.77	79.3	175.68	1.20
57	G3565	113.97	22.60	40.0	186.08	1.27
58	G3566	114.48	22.53	10.7	235.56	1.61
59	G3567	114.28	22.57	26.0	202.60	1.39
60	G3570	114.24	22.72	78.3	170.85	1.17
61	G3630	114.11	22.59	47.0	200.53	1.37
62	G3634	114.01	22.55	42.3	165.09	1.13
63	G3635	113.93	22.68	64.4	158.25	1.08
64	G3636	113.80	22.66	2.8	167.53	1.15
65	G3640	114.53	22.48	19.3	241.84	1.65
66	G3641*	113.94	22.50	19.6	146.39	1.00
67	G3643*	113.84	22.56	14.5	145.01	0.99
68	G3645*	114.03	22.52	2.3	148.46	1.02
69	G3649	114.20	22.68	73.0	164.80	1.13
70	G3659	114.19	22.57	652.8	197.44	1.35
71	G3661	114.21	22.71	189.0	156.98	1.07

(Continued)

**Table 3.** Continued.

No.	Station ID	Lon (°E)	Lat (°N)	Elevation (m)	Mean annual maximum 24-hour rainfall amount (mm)	OIF
72	G3666	114.56	22.56	11.0	221.50	1.51
73	G3674	114.56	22.48	154.8	196.80	1.35
74	G3704*	113.82	22.55	21.8	132.86	0.91
75	G3720	113.95	22.55	39.0	159.59	1.09
76	G3722	113.95	22.79	46.0	141.33	0.97
77	G3723	114.30	22.60	27.0	194.65	1.33
78	G3724	114.54	22.56	53.0	206.91	1.41
79	G3725	114.49	22.48	31.0	257.89	1.76
80	G3726	114.21	22.58	903.3	157.56	1.08
81	G3727	113.94	22.73	30.0	138.44	0.95
82	G3728	113.88	22.74	64.0	153.31	1.05
83	G3730	114.36	22.61	29.0	190.18	1.30
84	G3731	114.40	22.70	51.0	194.90	1.33
85	G3732	114.08	22.73	46.0	154.46	1.06
86	G3733	113.86	22.67	73.0	152.94	1.05
87	G3734	114.21	22.56	80.0	221.26	1.51
88	G3737	114.18	22.66	88.3	176.15	1.20
89	G3739	114.09	22.62	105.0	171.21	1.17
90	G3740	114.01	22.56	93.0	161.75	1.11
91	G3742	114.24	22.58	56.0	200.96	1.37
92	G3743	114.15	22.66	59.0	198.20	1.36
93	G3746	113.79	22.69	11.0	156.54	1.07
94	G3747	114.10	22.54	13.0	171.91	1.18
95	G3748	114.26	22.76	97.0	163.11	1.12
96	G3749	114.36	22.67	66.0	183.60	1.26
97	G3751	114.07	22.63	90.0	174.49	1.19
98	G3752	114.02	22.53	19.0	150.63	1.03
99	G3753	114.30	22.68	71.0	197.49	1.35
100	G3754	114.36	22.71	53.0	180.30	1.23
101	G3756	113.86	22.80	10.0	163.55	1.12
102	G3758	114.18	22.64	66.0	169.74	1.16
103	G3759	113.88	22.55	8.0	154.96	1.06
104	G3760	114.23	22.69	47.0	163.78	1.12
105	G3761	114.07	22.57	31.0	171.05	1.17
106	G3762	114.43	22.62	34.0	193.31	1.32
107	G3765	113.89	22.59	30.0	161.19	1.10
108	G3766	113.97	22.62	47.0	168.18	1.15
109	G3768	113.84	22.62	2.0	157.78	1.08

Note: \*Selected base rain stations.

and Table 2. The elevation and slope gradient are derived from a 2.5 m-resolution AW3D digital terrain model, and the soil thickness is taken empirically from a simple regression function between slope angle and soil thickness (Gao, Zhang, and Chen 2015). Geologically, the study area is underlain by granitic rocks, metamorphic rocks, alluvial deposits, and marine deposits, and over 70% of the hilly area is underlain by granitic rocks. For simplicity, the study area is divided into two zones, i.e. urban area with hard surface and

vegetated land. The material parameters are distinguished for the two zones, as summarised in Table 2, which have been calibrated by Zhou, Gao, and Zhang (2019). For each cell, area reduction factor and width reduction factors are assigned according to the shape of buildings (Figure 3) identified from satellite images. Since public data on drainage networks is limited, the equivalent drainage method is used in this study to approximate the capacity of the urban drainage system. The infiltration adjustment factors  $K$  in different

**Table 4.** Designated rainstorm scenarios and corresponding infiltration adjustment factors.

No.	Scenario	Description	Maximum 24-hour rainfall amount (mm)	Infiltration adjustment factor, $K$
1	2008 storm	Hourly rainfall process recorded at Shenzhen rain station (corresponding to 10-year return period); Spatially uniform	280	1.25
2	100-year storm	Scaling the process of the 2008 rainstorm to a 100-year return period for the 24-hour rainfall amount; Spatially uniform	462	2
3	1000-year storm	Scaling the process of the 2008 rainstorm to a 1000-year return period for the 24-hour rainfall amount; Spatially uniform	631	2.5
4	85% of local 24-hour PMP	85% of local PMP centred at Tanglang Mountain (114.025°E, 22.585°N); The temporal pattern is the same as the 2008 rainstorm; Spatially varying	934–1225 (1044 on average)	4

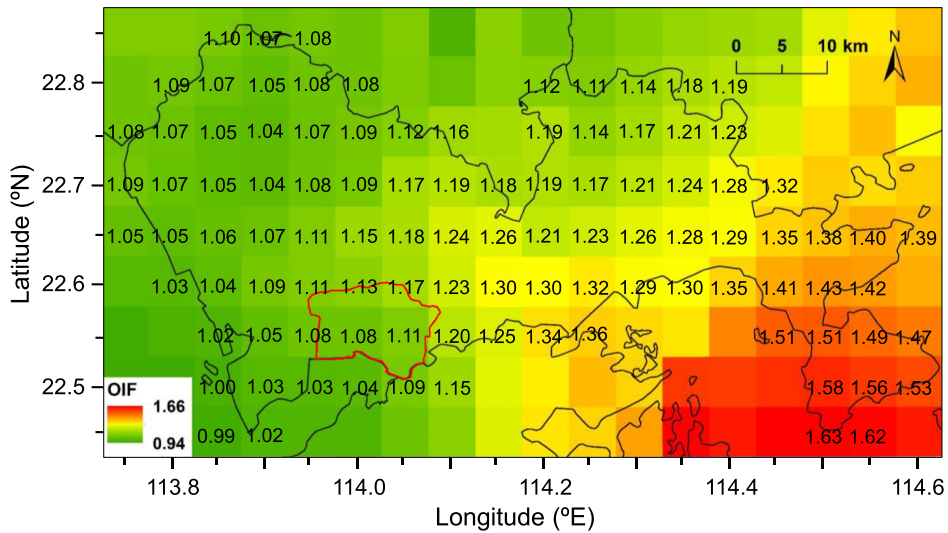


**Figure 5.** Gridded 24-hour orographic intensification factors for Shenzhen.

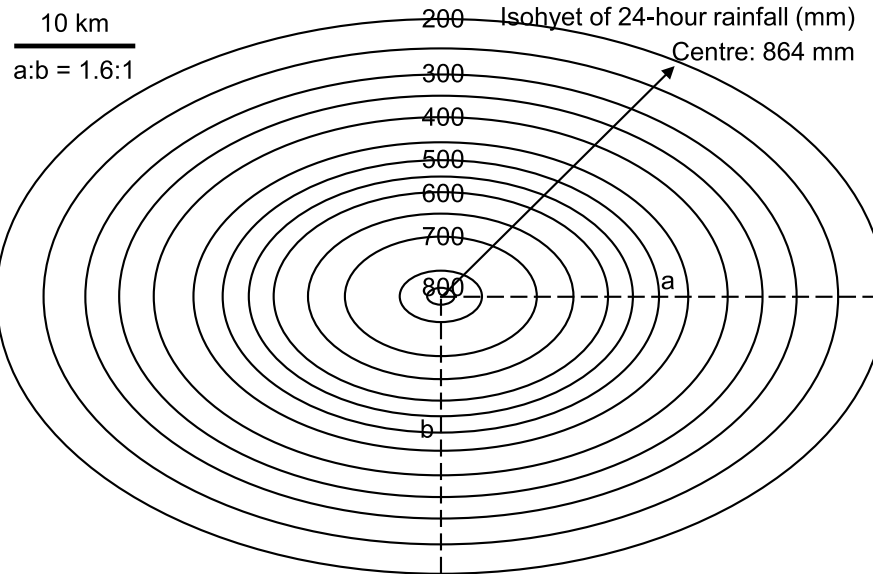


**Figure 6.** Convergence component pattern of rainfall.

rainstorm scenarios ([Table 4](#)) are calibrated with a flood model with a physically based drainage network built for the Kowloon area in Hong Kong, the technical details of which can be found in [Qiang et al. \(2021b\)](#).

A stressful storm in the past 20 years, i.e. 13–14 June 2008 storm, is used to validate the developed EDDA model. The storm centre was in Bao'an District, with the maximum cumulative rainfall amount exceeding 600 mm, corresponding to a return period of 50~100 years ([Chai 2010](#)). The rainfall process ([Figure 4\(a\)](#)) recorded at the Shenzhen Rain Station (as marked in [Figure 2\(b\)](#)) is utilised, which is regarded as spatially uniform in the study area. The maximum 24-hour rainfall amount was 280 mm,

the return period of which was about 10 years ([Chai 2010](#)). The simulated landslide and flooding spots in this storm are shown in [Figure 4\(b\)](#) and (c), respectively. These locations are well within the high hazard-prone areas identified from a landslide susceptibility map ([Xing et al. 2021](#)) ([Figure 4\(b\)](#)) and a flood hazard map ([Sarica et al. 2021](#)) ([Figure 4\(d\)](#)) developed based on historical hazard records in Shenzhen. Specifically, the landslide susceptibility corresponding to the simulated slope failure locations ranges from 0.54–0.98, with an average to be 0.85; and 78% of simulated flooding spots with water depth larger than 1 m fall in the moderate to high susceptibility regions in the flood hazard map. The

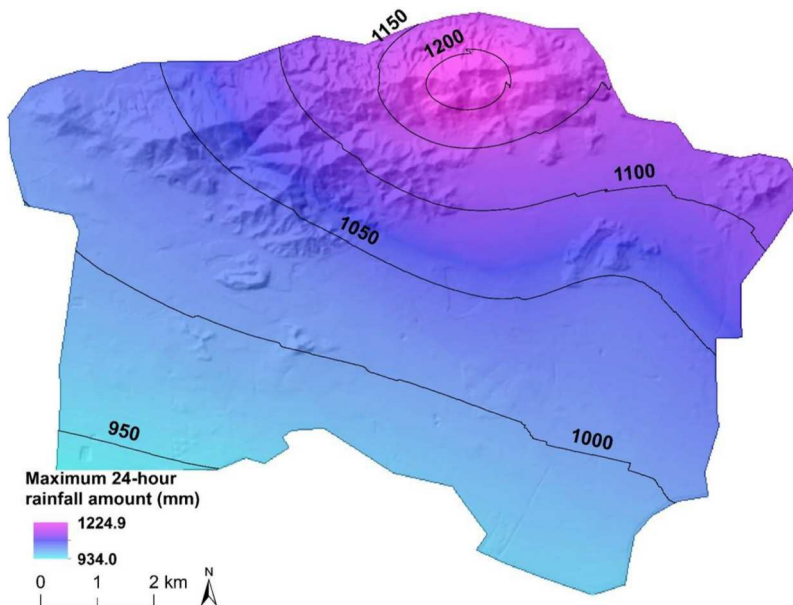


**Figure 7.** Maximum 24-hour rainfall amount of the 85% PMP scenario.

**Table 5.** Summary of simulated hazards under the designated rainstorm scenarios.

Rainstorm scenario	1	2	3	4
Number of slope failures	121	200	251	318
Volume of slope failure (m <sup>3</sup> )	80,699	163,274	224,597	311,034
Area affected by landslides (km <sup>2</sup> )	0.45	0.63	0.81	0.78
Area affected by debris flows (km <sup>2</sup> )	0.10	0.30	0.41	0.67
Flooding area (km <sup>2</sup> )	9.57	16.70	22.25	32.38

high consistency in spatial patterns of both landslide and flood hazards indicates the reliability of the developed numerical model.

### 3.3. Probable maximum precipitation

Estimating the PMP of the study area is critical for extreme storm design. In the content of the storm transposition method, the orographic intensification factors of Shenzhen should be determined first. The hourly rainfall data from 2013–2020 at 109 rain stations in Shenzhen (Figure 2(a)) are collected from the Meteorological Bureau of Shenzhen Municipality. To obtain the 24-hour annual maximum rolling rainfall series for each rain station, invalid data and missing data are replaced by 0 for simplicity and the maximum values are picked

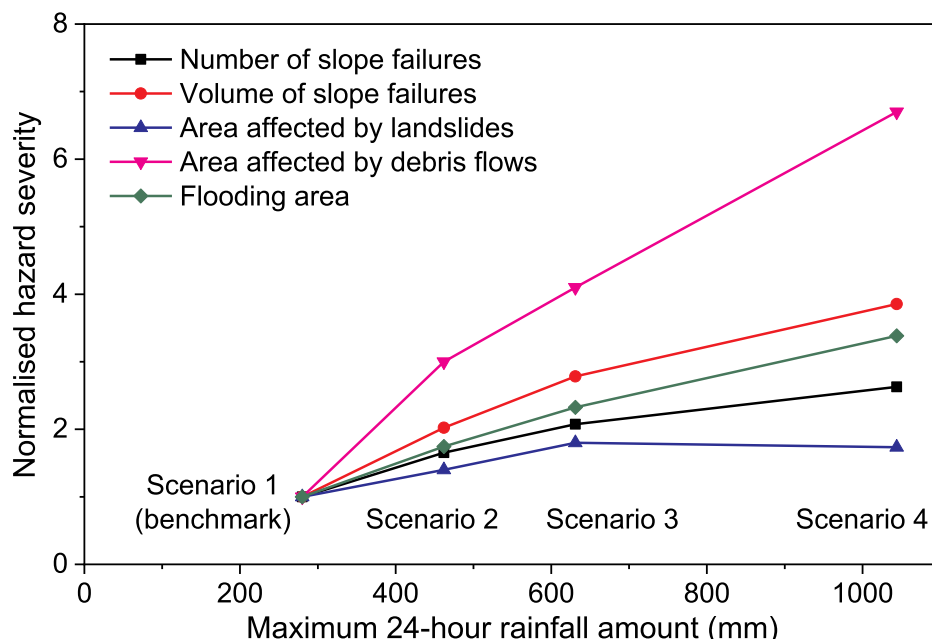


**Figure 8.** Variation of simulated hazard severity with rainstorm intensity.

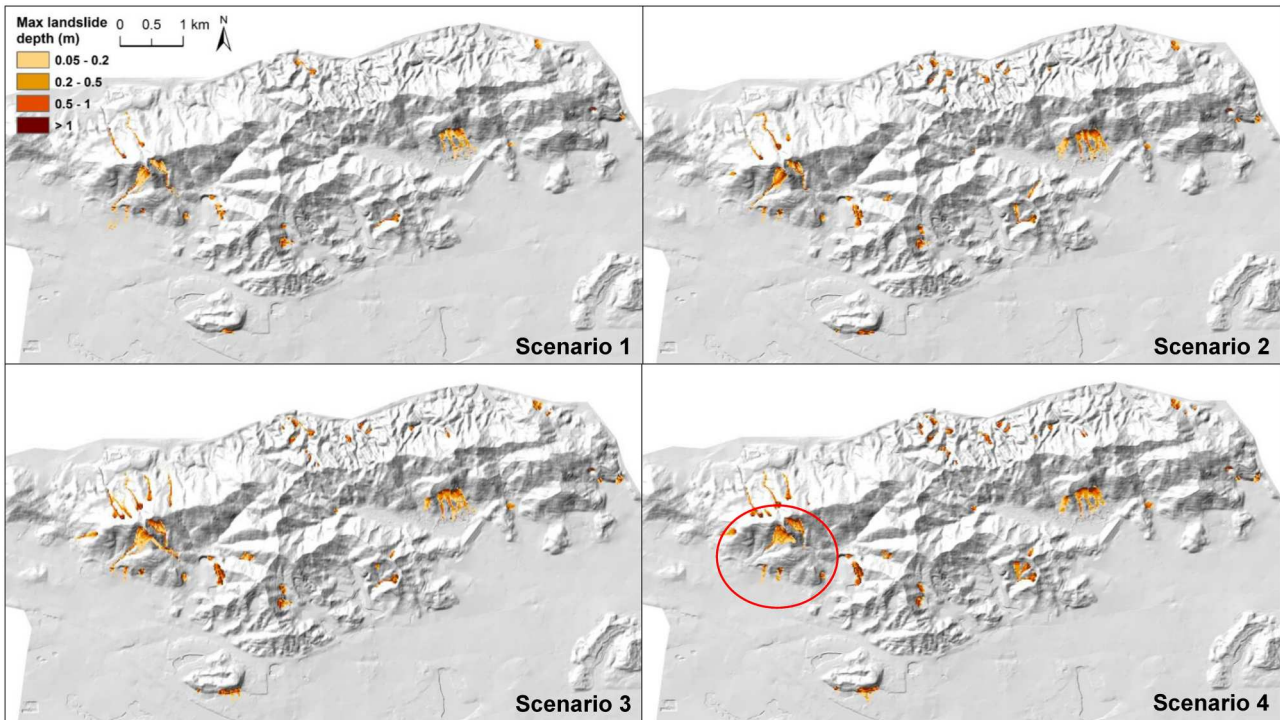


**Figure 9.** Simulated maximum landslide depths in the four rainstorm scenarios.

up by a 24-hour moving window. As shown in Figure 2(a), the maximum 24-hour rainfall amount ranges from 133 mm on the west coast to 258 mm in the east hilly region of the Dapeng Peninsula. Seven stations

(as marked in Figure 2(a)) in the flat coastal area in the westerly moisture inflow direction are selected as the base stations to calculate  $R_{0,T}(x)$  in Equation (4). The orographic intensification factor of each rain

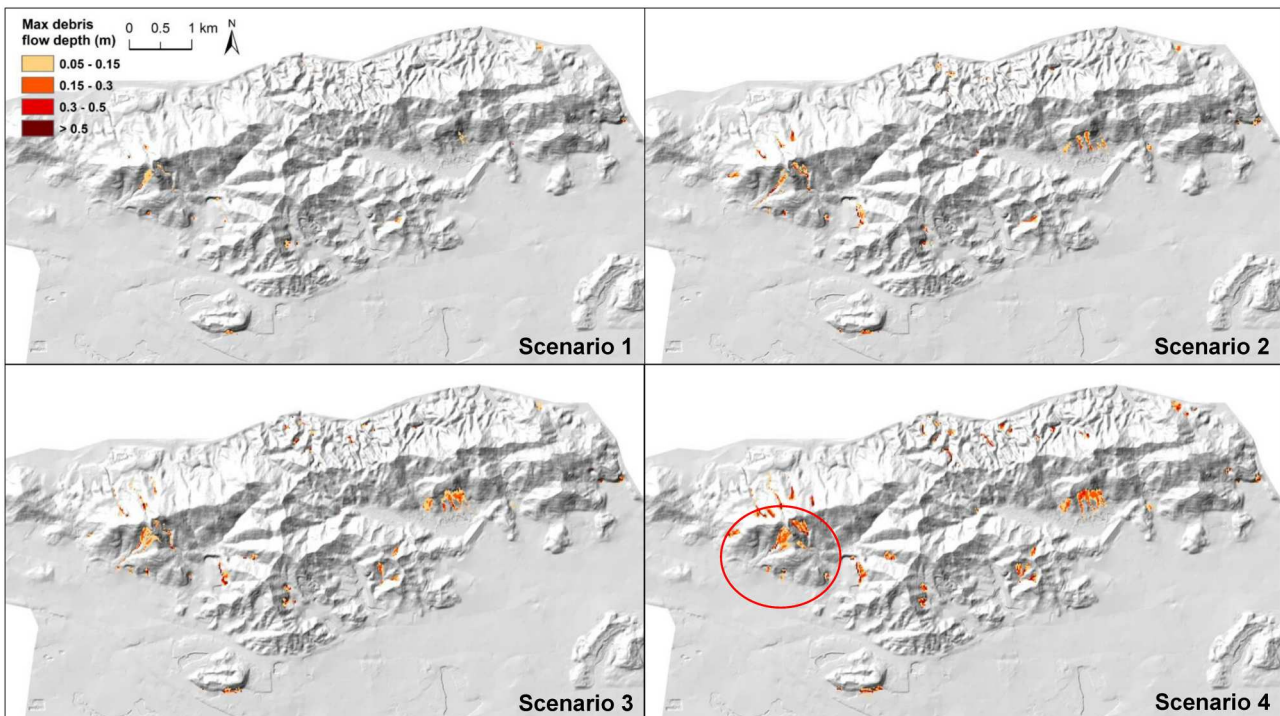


**Figure 10.** Simulated maximum debris flow depths in the four rainstorm scenarios.

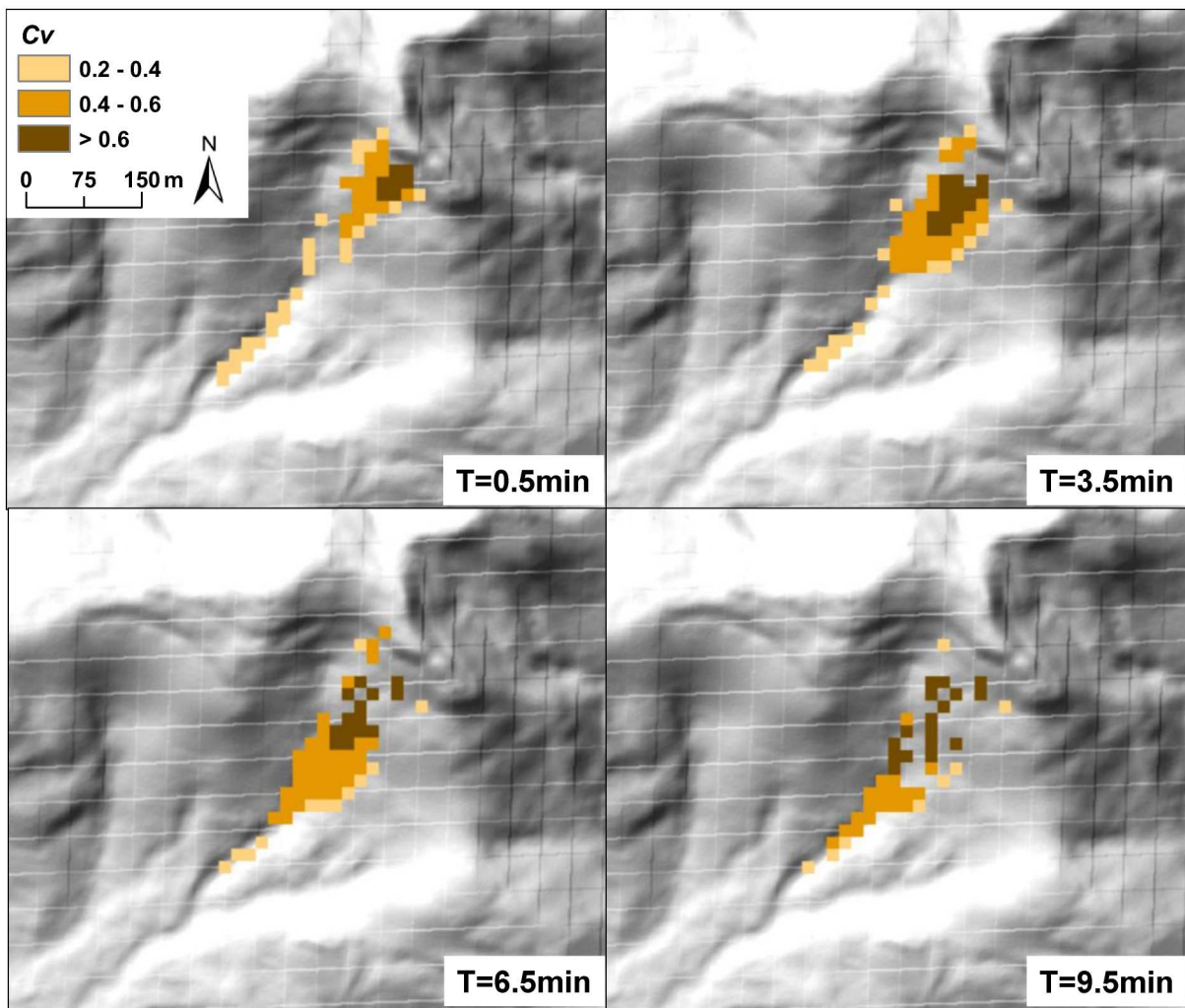


**Figure 11.** Hazard transformation after a slope failure in the 85% PMP scenario ( $T$  is the time after slope failure).

station calculated from Equation (4) is provided in Table 3. Then a gridded frame covering the entire Shenzhen at a resolution of  $5\text{ km} \times 5\text{ km}$  is obtained through spatial interpolation, as shown in Figure 5. The estimated 24-hour orographic intensification factors for Shenzhen range from 0.99–1.63.

It is reasonable to assume that Shenzhen, Hong Kong and Taiwan are meteorologically homogeneous in terms of typhoon-prone area in the northwest pacific region (Chong and Lee 2015; Lin 2015). From the surveyed outstanding storms in Southeast China (Lin 2015), the 2009 Typhoon Morakot in Taiwan is the most severe storm within this region regarding its intensity and consequence and is thus selected as a target storm for transposition. Following Lin (2015), a generalised convergence component pattern of rainfall is suggested (Figure 6), represented by isohyets of a group of concentric ellipses with an aspect ratio of 1.6 and the highest rainfall at the centre of 864 mm (derived from Typhoon Morakot). The convergence component is

superposed on the grid of the orographic intensification factor of the study area to calculate the embryonic PMP portion. To consider the most severe situation, the storm is assumed to be centred at Tanglang Mountain ( $114.025^\circ\text{E}$ ,  $22.585^\circ\text{N}$ , Figure 2(b)) where the OIF is about 1.136 after interpolation. The centre value of the embryonic PMP in the study area is calculated as 982 mm.

With respect to the calculation of moisture maximisation ratio, the precipitable water of Typhoon Morakot in Taiwan ( $W_S$ ) can be estimated from the representative storm dew point observed before the typhoon, which was  $24^\circ\text{C}$  in Lin (2015), and the corresponding precipitable water was 74.3 mm (WMO 2009 – Table A.1.3). As the dew point data available in Shenzhen are limited, the maximum precipitable water in Shenzhen ( $W_M$ ) is estimated using the 100-year return period event from frequency analysis with the dew point data from 2014–2018 recorded at five base stations in the moisture inflow direction. The annual 12-hour

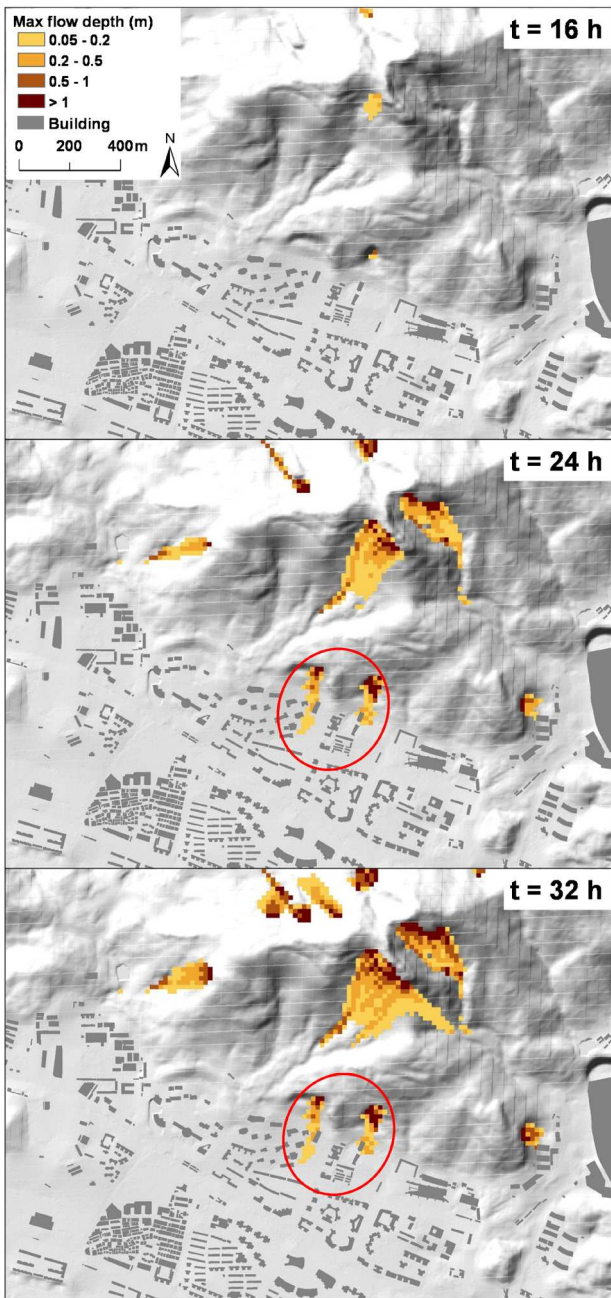


**Figure 12.** Progression of areas affected by landslides and debris flows in the 85% PMP scenario.

maximum persisting dew points occurred from a period of 24 hours before the onset of rainstorms at each station are calculated. Given the short observation period, data from all five stations are pooled together when carrying out frequency analysis. The generalised extreme value distribution is adopted to fit the 12-hour maximum persisting dew point using the maximum likelihood estimation. The 100-year return period 12-hour persisting dew point in Shenzhen is estimated as 28.5°C, and the corresponding precipitable water is 109.1 mm (WMO 2009 – Table A.1.3). Therefore, the

moisture maximisation ratio is calculated as  $r_m = 109.1/74.3 = 1.468$ , which is slightly larger than that estimated for Hong Kong (i.e. 1.304). Eventually, the PMP for the study area is obtained by multiplying the embryonic PMP by  $r_m$ , leading to a centre value being 1441 mm at Tanglang Mountain.

#### 4. Multi-hazard stress testing

##### 4.1. Designated rainstorm scenarios

Apart from the 2008 Shenzhen rainstorm (Scenario 1, 10-year return period) used for model verification and benchmarking, three more extreme rainstorm scenarios are designed to conduct multi-hazard stress testing, as summarised in Table 4. In Scenarios 2 and 3, the 2008 rainstorm is scaled to levels of 100-year and 1000-year return periods according to Chai (2010), with the maximum 24-hour rainfall amount to be 462 and 631 mm, respectively. Different to Scenarios 1–3 where the rainstorms are spatially uniform, Scenario 4 follows the spatial distribution of the 24-hour local PMP (scaled to 85% with the orientation of convergence component being 0°) and the temporal pattern of the 2008 rainstorm. Figure 7 shows the distribution of the maximum 24-hour rainfall amount for this scenario, which varies from 934 mm–1225 mm, with an average value of 1044 mm. This scenario represents a very extreme rainstorm, which was also adopted in the previous hazard analysis for Hong Kong (Zhou, Gao, and Zhang 2019).

Hazards in the four rainstorm scenarios are simulated using EDDA. Table 5 summarises the simulated results in terms of five key indicators, i.e. number and volume of slope failures, areas affected by landslides and debris flows, and flooding area. Note that, in this study, areas affected by landslides and debris flows are defined as regions with a maximum landslide (or debris flow) depth larger than 0.05 m, and the flooding area is defined as regions with a maximum flooding depth larger than 0.15 m. Figure 8 shows the variation of simulated hazard severity with respect to the maximum 24-hour rainfall amount, where all the results are normalised by the respective benchmark values of Scenario 1 for comparison.

##### 4.2. Landslides and debris flows in hilly regions

Figures 9 and 10 show the simulated landslides and debris flows, respectively, in the four rainstorm scenarios. Landslides and debris flows mostly take place in the hilly Tanglang Mountain region and rarely occur at Lianhua Hill and Bijia Hill, where the slope angles are smaller than 30°. The number and volume of slope failures grow

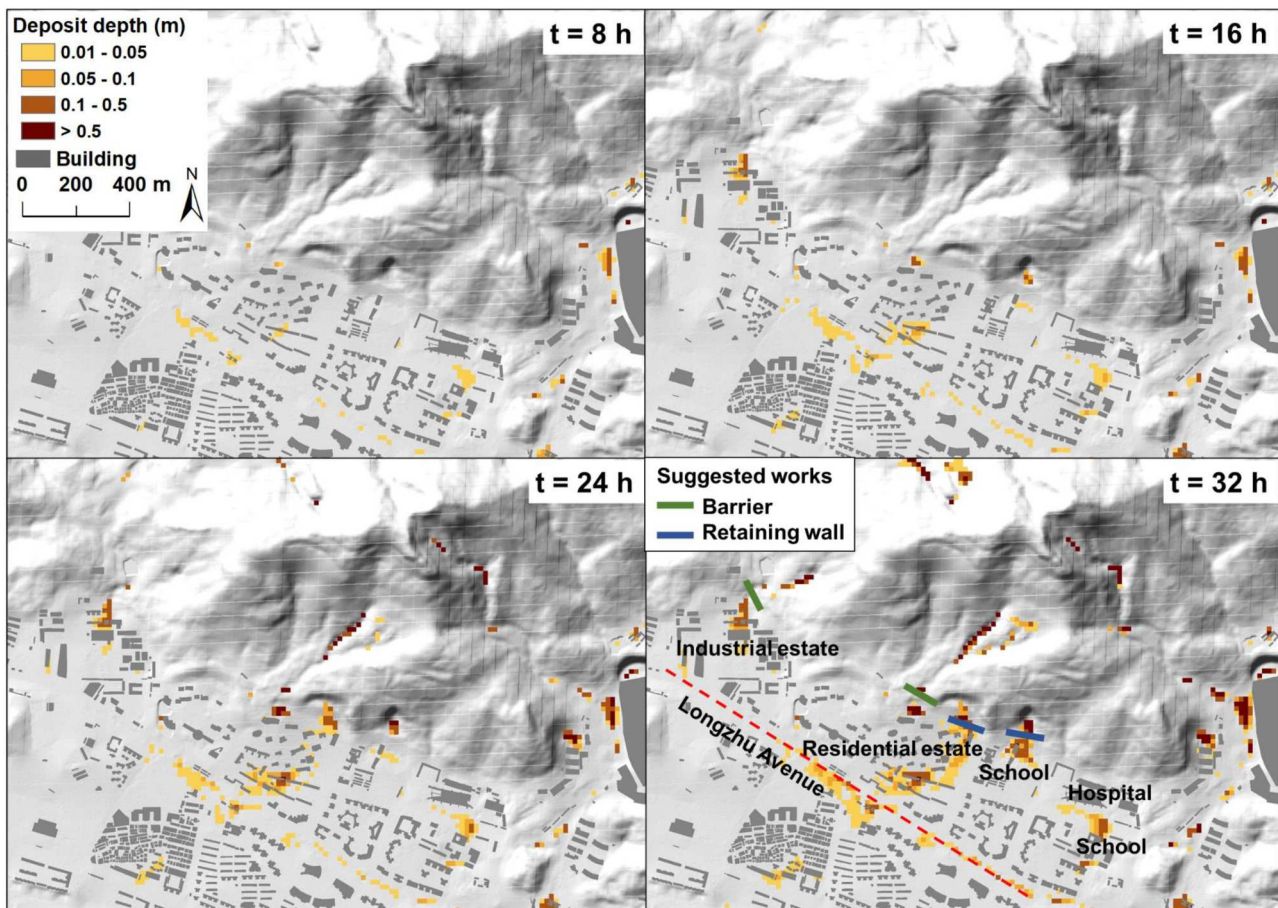


**Figure 13.** Progression of deposit depths in the 85% PMP scenario and suggested engineering works for landslide risk mitigation.

with the rainstorm intensity in a linear trend from Scenarios 1–3, and remain increasing in Scenario 4 (i.e. 85% PMP) but with a smaller rate. It implies that the growth rate of the severity of slope failures may slow down when the rainstorm becomes very extreme. The area affected by debris flows is very limited in Scenario 1, and gradually grows with the increase in rainstorm intensity. Compared to Scenario 3, areas affected by landslides decrease slightly but areas affected by debris flows increase significantly in Scenario 4, which indicates that more slope failure masses are transformed from landslides to debris flows. For the two extreme rainstorm scenarios (i.e. Scenarios 3 and 4), the areas affected by landslides and debris flows will be 0.85 and 0.88 km<sup>2</sup>, respectively, which are about 3.0% and 3.1% of hilly regions.

Note that both landslides and debris flows can occur during an intense rainstorm, and the morphology of flow changes during the motion with the processes of entrainment, erosion and deposition. Figure 11 shows a detailed variation process of the volumetric solid concentration of the flow after a slope failure happens in the 85% PMP rainstorm scenario. From  $T = 0.5$  min to  $T = 6.5$  min, the landslide

mass ( $C_v > 0.6$ ) moves from the location where the slope failure happens to the downstream of the catchment along the drainage line, and the lower edge of the landslide mass gradually mixes with surface runoff and transforms to debris flow ( $0.2 < C_v < 0.6$ ). At  $T = 9.5$  min, areas with  $C_v$  larger than 0.2 become discontinuous, which indicates that most of the flow has become clear flood water.

As shown in Figures 9 and 10, the southwest foot of Tanglang Mountain as marked is most prone to landslides and debris flows. This location is close to the urban region and the hazards may lead to severe consequences. Therefore, the hazard maps simulated in the 85% PMP scenario at this location are zoomed in to learn about the affected area in detail. Figures 12 and 13 demonstrate the development of areas affected by landslides and debris flows and the development of soil deposits, respectively. Since protective measures for slopes are not considered in the current model, landslide masses caused by slope failures at steep hillsides of the mountain foot (circled in Figure 12) will enter downstream residential areas (Figure 13). There would be many mass deposits along Longzhu Avenue and in

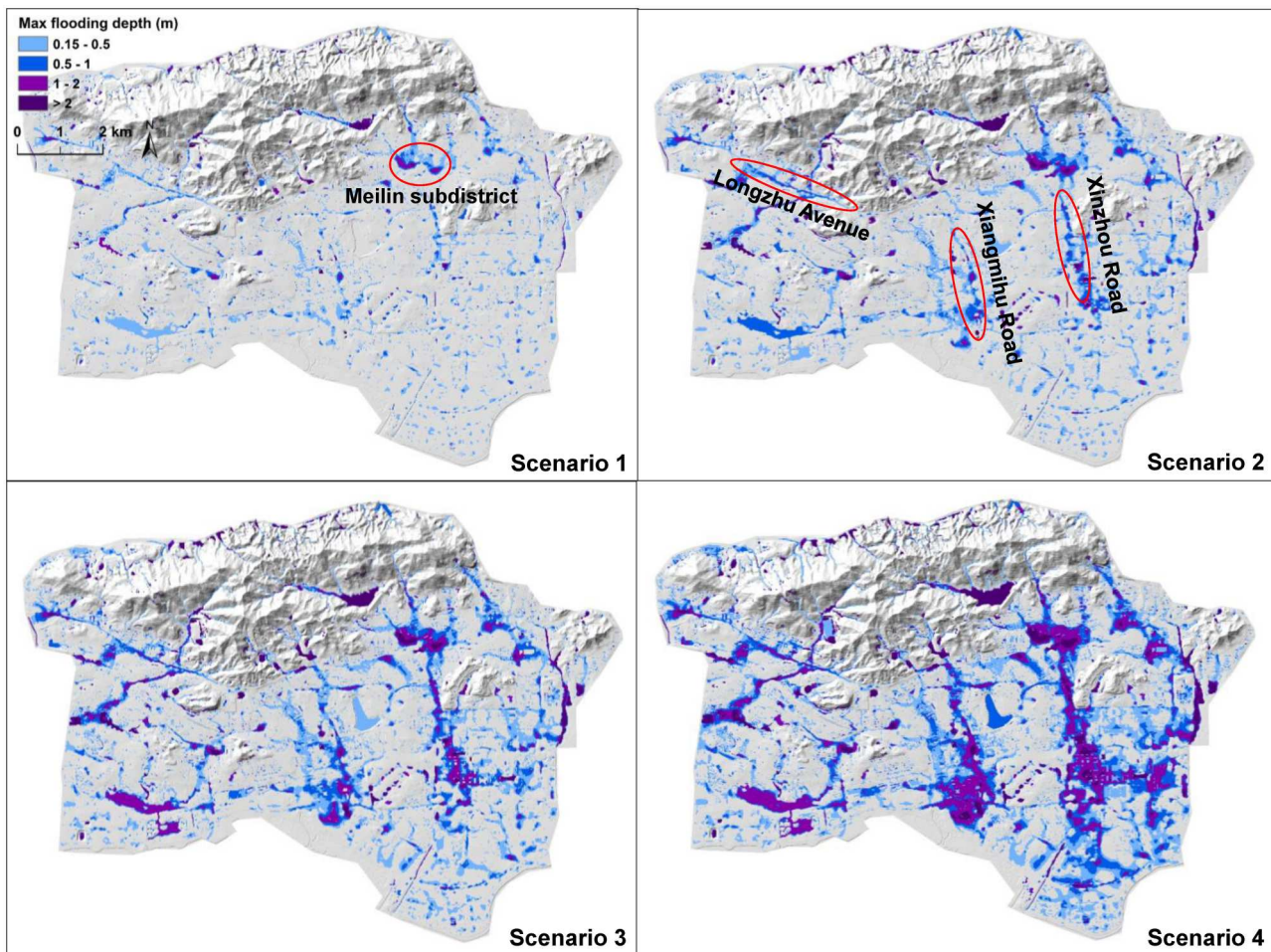


**Figure 14.** Simulated maximum flooding depths in the four rainstorm scenarios.

the residential communities, affecting one industrial estate, one residential estate, two schools and one hospital. Landslide prevention and mitigation works are necessary to protect these high-risk areas against extreme rainstorms. Considering the characteristics of hazard and terrain, two barriers and two retaining walls are suggested with higher priority, with respective locations marked in Figure 13(d). In addition, some deposits still hang on the hillslopes with depths even larger than 0.5 m. If they cannot be treated in time, new debris flows may form in subsequent rainstorms and affect the urban regions again.

#### 4.3. Flooding in flat built-up regions

The developed urban regions can be flooded extensively under extreme storms. Figure 14 compares the simulated flood maps in the four rainstorm scenarios. Areas with maximum simulated water depths larger than 0.15 and 1 m are identified as flooded and severely flooded, respectively. The influence of flooding is more extensive compared to landslides and debris flows. The

flooding severity grows with the increasing rainstorm intensity. In Scenario 1, the inundation depths of most flooding areas are smaller than 0.5 m. Sporadic flooding spots with inundation depths larger than 0.5 m occur at low-lying areas such as the Meilin subdistrict at the lower reaches of the catchments. In Scenario 2, more continuous inundation areas occur along some roads, such as the Xiangmihu Road, Xinzhou Road and Longzhu Avenue. In the two extreme rainstorm scenarios, the scale of flooding expands further, with much broader areas severely flooded. The flooding area reaches 22.25 and 32.38 km<sup>2</sup> in Scenarios 3 and 4, respectively, which means 23.5% and 34.2% of the study area are flooded. Moreover, severely flooded areas are 4.65 and 9.23 km<sup>2</sup> in the two extreme rainfall scenarios, respectively, which account for 4.9% and 9.8% of the study area. Although the spatial variability of the drainage capacity and the flood mitigation facilities are not considered in the equivalent drainage method adopted, the simulated flooding maps reflect the vulnerable regions necessary to enhance mitigation measures when facing future extreme rainstorm events.

Engineering measures for temporary water storage (e.g. underground storage tanks) and for speeding up the drainage of stormwater (e.g. pumping stations) are necessary for those inundation-prone areas to reduce flooding risk.

## 5. Conclusions

This study develops an integrated multi-hazard stress testing method under extreme rainstorms in the metropolitan region of Shenzhen. The major conclusions from this study and recommendations for future works are as follows:

- (1) The PMP of the study area is estimated using the storm transposition method considering orographic intensification and moisture maximisation, with the centre peak amount being 1441 mm in 24 hours at Tanglang Mountain. Several rainstorms are designed as stress scenarios for multi-hazard stress testing, including two extreme events corresponding to a 1000-year return period and 85% PMP.
- (2) An integrated numerical model, EDDA, is utilised to simulate the processes of initiation, propagation and transformation of landslides, debris flows and flooding in a unified manner, in which the urban drainage network can be flexibly modelled using either a physically based method or an equivalent drainage method. Hotspots of different hazard types are identified and their influences are evaluated.
- (3) Landslides and debris flows will happen in the hilly regions of Tanglang Mountain. With the increase in rainstorm intensity, more landslides will transform into debris flows with more surface runoff. Under the 1000-year return period and 85% PMP rainstorms, the deposit depths can be large in the urban areas near the southwest foot of Tanglang Mountain, which can affect many residential communities. By contrast, extensive inundation will happen in the flat built-up regions under the 1000-year return period and 85% PMP rainstorms, with 23.5% and 34.2% of the study area flooded, respectively.
- (4) The hazard mitigation measures, such as protective engineering works for slopes and strategic storm-water storage facilities, are not yet considered in the simulation. To conduct a complete risk-informed stress test, influences of these measures need to be incorporated in the multi-hazard analysis model in the future to verify the effectiveness of the current and planned hazard mitigation systems against extreme rainstorms.

## Disclosure statement

No potential conflict of interest was reported by the author(s).

## Funding

This work was supported by the National Key R&D Program of China: [Grant Number 2021YFC3001000]; the National Natural Science Foundation of China: [Grant Number 52025094, 52409136]; the Research Grants Council of the Hong Kong SAR: [Grant Number T22-606/23-R]; the Hetao Shenzhen-Hong Kong Science and Technology Innovation Cooperation Zone: [Grant Number HZQB-KCZYB-2020083].

## ORCID

Te Xiao  <http://orcid.org/0000-0003-4935-892X>

## References

- Ba, R., Q. Deng, Y. Liu, R. Yang, and H. Zhang. 2021. "Multi-hazard Disaster Scenario Method and Emergency Management for Urban Resilience by Integrating Experiment-Simulation-Field Data." *Journal of Safety Science and Resilience* 2 (2): 77–89. <https://doi.org/10.1016/j.jnlssr.2021.05.002>.
- Bout, B., L. Lombardo, C. J. van Westen, and V. G. Jetten. 2018. "Integration of Two-Phase Solid Fluid Equations in a Catchment Model for Flashfloods, Debris Flows and Shallow Slope Failures." *Environmental Modelling & Software* 105:1–16. <https://doi.org/10.1016/j.envsoft.2018.03.017>.
- Cascini, L., S. Cuomo, A. Di Mauro, M. Di Natale, S. Di Nocera, and F. Matano. 2021. "Multidisciplinary Analysis of Combined Flow-Like Mass Movements in a Catchment of Southern Italy." *Georisk: Assessment and Management of Risk for Engineered Systems and Geohazards* 15 (1): 41–58. <https://doi.org/10.1080/17499518.2019.1674339>.
- Chai, Y. 2010. "Analysis on the Return Period of the '6.13' Heavy Rain in 2008 in Shenzhen." *China Rural Water and Hydropower* 8:70–73. in Chinese.
- Chen, H. X., and L. M. Zhang. 2015. "EDDA 1.0: Integrated Simulation of Debris Flow Erosion, Deposition and Property Changes." *Geoscientific Model Development* 8 (3): 829–844. <https://doi.org/10.5194/gmd-8-829-2015>.
- Chong, S. N., and T. C. Lee. 2015. "Regional Frequency Analysis of Extreme Rainfall in Hong Kong, Macao and Guangzhou." HKO Reprint No. 1164. Hong Kong Observatory, HKSAR.
- Clarke, M. L., and H. M. Rendell. 2006. "Hindcasting Extreme Events: The Occurrence and Expression of Damaging Floods and Landslides in Southern Italy." *Land Degradation & Development* 17 (4): 365–380. <https://doi.org/10.1002/ldr.743>.
- Destro, E., W. Ampsonah, E. I. Nikolopoulos, L. Marchi, F. Marra, D. Zoccatelli, and M. Borga. 2018. "Coupled Prediction of Flash Flood Response and Debris Flow Occurrence: Application on an Alpine Extreme Flood

- Event." *Journal of Hydrology* 558:225–237. <https://doi.org/10.1016/j.jhydrol.2018.01.021>.
- Dilley, M., R. S. Chen, U. Deichmann, A. L. Lerner-Lam, and M. Arnold. 2005. *Natural Disaster Hotspots: A Global Risk Analysis*. Washington D.C., USA: The World Bank.
- Du, H., K. Fei, J. Wu, and L. Gao. 2024. "An Integrative Modelling Framework for Predicting the Compound Flood Hazards Induced by Tropical Cyclones in an Estuarine Area." *Environmental Modelling & Software* 175:105996. <https://doi.org/10.1016/j.envsoft.2024.105996>.
- Fan, X., F. Yang, S. Siva Subramanian, Q. Xu, Z. Feng, O. Mavrouli, M. Peng, C. Ouyang, D. J. Jansen, and R. Huang. 2020. "Prediction of a Multi-Hazard Chain by an Integrated Numerical Simulation Approach: The Baige Landslide, Jinsha River, China." *Landslides* 17 (1): 147–164. <https://doi.org/10.1007/s10346-019-01313-5>.
- FLO-2D. 2018. *FLO-2D Pro Version: Two-Dimensional Flood Routing Model - Storm Drain Manual*. Nutrioso, AZ, USA: FLO-2D Software, Inc.
- Gao, L., H. Du, H. Huang, L. Zhang, and P. Zhang. 2023a. "Modelling the Compound Floods upon Combined Rainfall and Storm Surge Events in a low-Lying Coastal City." *Journal of Hydrology* 627:130476. <https://doi.org/10.1016/j.jhydrol.2023.130476>.
- Gao, L., L. M. Zhang, and H. X. Chen. 2015. "Likely Scenarios of Natural Terrain Shallow Slope Failures on Hong Kong Island Under Extreme Storms." *Natural Hazards Review* 18 (1): B4015001. [https://doi.org/10.1061/\(ASCE\)NH.1527-6996.0000207](https://doi.org/10.1061/(ASCE)NH.1527-6996.0000207).
- Gao, L., L. Zhang, Y. Hong, H. X. Chen, and S. J. Feng. 2023b. "Flood Hazards in Urban Environment." *Georisk: Assessment and Management of Risk for Engineered Systems and Geohazards* 17 (2): 241–261. <https://doi.org/10.1080/17499518.2023.2201266>.
- Gao, L., L. Zhang, X. Li, and S. Zhou. 2019. "Evaluating Metropolitan Flood Coping Capabilities Under Heavy Storms." *Journal of Hydrologic Engineering* 24 (6): 05019011. [https://doi.org/10.1061/\(ASCE\)HE.1943-5584.0001793](https://doi.org/10.1061/(ASCE)HE.1943-5584.0001793).
- Guo, Z., B. Tian, J. He, C. Xu, T. Zeng, and Y. Zhu. 2023. "Hazard Assessment for Regional Typhoon-Triggered Landslides by Using Physically-Based Model – a Case Study from Southeastern China." *Georisk: Assessment and Management of Risk for Engineered Systems and Geohazards* 17 (4): 740–754. <https://doi.org/10.1080/17499518.2023.2188465>.
- Han, T., B. Lin, J. Wu, and X. Wei. 2024. "Three-dimensional Stability Analysis of two-Layer Slope Based on GIS Under Rainfall Conditions." *Georisk: Assessment and Management of Risk for Engineered Systems and Geohazards* 18 (2): 423–446. <https://doi.org/10.1080/17499518.2024.2302134>.
- He, J., Y. Qiang, H. Luo, S. Zhou, and L. Zhang. 2021. "A Stress Test of Urban System Flooding upon Extreme Rainstorms in Hong Kong." *Journal of Hydrology* 597:125713. <https://doi.org/10.1016/j.jhydrol.2020.125713>.
- He, J., L. Zhang, T. Xiao, H. Wang, and H. Luo. 2023. "Deep Learning Enables Super-Resolution Hydrodynamic Flooding Process Modeling Under Spatiotemporally Varying Rainstorms." *Water Research* 239:120057. <https://doi.org/10.1016/j.watres.2023.120057>.
- Ho, K., S. Lacasse, and L. Picarelli. 2017. *Slope Safety Preparedness for Impact of Climate Change*. Balkema, The Netherlands: CRC Press.
- IPCC (Intergovernmental Panel on Climate Change). 2012. *Managing the Risks of Extreme Events and Disasters to Advance Climate Change Adaptation*. New York, USA: Cambridge University Press.
- Kappes, M. S., M. Keiler, K. von Elverfeldt, and T. Glade. 2012. "Challenges of Analyzing Multi-Hazard Risk: A Review." *Natural Hazards* 64 (2): 1925–1958. <https://doi.org/10.1007/s11069-012-0294-2>.
- Kumar, A., A. K. L. Asthana, R. S. Priyanka, R. Jayangondaperumal, A. K. Gupta, and S. S. Bhakuni. 2017. "Assessment of Landslide Hazards Induced by Extreme Rainfall Event in Jammu and Kashmir Himalaya, Northwest India." *Geomorphology* 284:72–87. <https://doi.org/10.1016/j.geomorph.2017.01.003>.
- AECOM, and B. Lin. 2015. "24-hour Probable Maximum Precipitation Updating Study." GEO Report No. 314. Geotechnical Engineering Office, HKSAR.
- Lin, B. 2017. "4-hour Probable Maximum Precipitation Updating Study in Hong Kong." GEO Report No. 331. Geotechnical Engineering Office, HKSAR.
- Lu, M., H. Wang, A. Sharma, and J. Zhang. 2024. "A Stochastic Rainfall Model for Reliability Analysis of Rainfall-Induced Landslides." *Georisk: Assessment and Management of Risk for Engineered Systems and Geohazards*, 1–15. <https://doi.org/10.1080/17499518.2024.2359957>.
- Lyu, H. M., and Z. Y. Yin. 2023. "An Improved MCDM Combined with GIS for Risk Assessment of Multi-Hazards in Hong Kong." *Sustainable Cities and Society* 91:104427. <https://doi.org/10.1016/j.scs.2023.104427>.
- O'Brien, J. S., P. Y. Julien, and W. T. Fullerton. 1993. "Two-Dimensional Water Flood and Mudflow Simulation." *Journal of Hydraulic Engineering* 119 (2): 244–261. [https://doi.org/10.1061/\(ASCE\)0733-9429\(1993\)119:2\(244\)](https://doi.org/10.1061/(ASCE)0733-9429(1993)119:2(244)).
- Oguz, E. A., R. E. Benestad, K. M. Parding, I. Depina, and V. Thakur. 2024. "Quantification of Climate Change Impact on Rainfall-Induced Shallow Landslide Susceptibility: A Case Study in Central Norway." *Georisk: Assessment and Management of Risk for Engineered Systems and Geohazards* 18 (2): 467–490. <https://doi.org/10.1080/17499518.2023.2283848>.
- Peng, M., and L. M. Zhang. 2012. "Analysis of Human Risks due to dam Break Floods – Part 2: Application to Tangjiashan Landslide dam Failure." *Natural Hazards* 64 (2): 1899–1923. <https://doi.org/10.1007/s11069-012-0336-9>.
- Peng, M., and L. M. Zhang. 2013. "Dynamic Decision Making for dam-Break Emergency Management–Part 1: Theoretical Framework." *Natural Hazards and Earth System Sciences* 13 (2): 425–437. <https://doi.org/10.5194/nhess-13-425-2013>.
- Qiang, Y., J. He, T. Xiao, W. Lu, J. Li, and L. Zhang. 2021a. "Coastal Town Flooding upon Compound Rainfall-Wave Overtopping-Storm Surge During Extreme Tropical Cyclones in Hong Kong." *Journal of Hydrology: Regional Studies* 37:100890. <https://doi.org/10.1016/j.ejrh.2021.100890>.
- Qiang, Y., L. Zhang, J. He, T. Xiao, H. Huang, and H. Wang. 2021b. "Urban Flood Analysis for Pearl River Delta Cities

- Using an Equivalent Drainage Method upon Combined Rainfall-High Tide-Storm Surge Events." *Journal of Hydrology* 597:126293. <https://doi.org/10.1016/j.jhydrol.2021.126293>.
- Qiang, Y., L. Zhang, and T. Xiao. 2020. "Spatial-temporal Rain Field Generation for the Guangdong-Hong Kong-Macau Greater Bay Area Considering Climate Change." *Journal of Hydrology* 583:124584. <https://doi.org/10.1016/j.jhydrol.2020.124584>.
- Ramakrishnan, M., P. K. Sharma, A. D. Roshan, A. S. Pisharady, M. M. Raj, P. Chithira, J. Arul, and L. R. Bishnoi. 2022. "Application of External Flood Probabilistic Safety Assessment Methodology to Prototype Fast Breeder Reactor." *Georisk: Assessment and Management of Risk for Engineered Systems and Geohazards* 16 (4): 782–797. <https://doi.org/10.1080/17499518.2022.2144636>.
- Regier, E., J. Naughton, and W. McDonald. 2022. "Transposing Flood Risk from Extreme Rainfall Events: A Case Study of Hurricane Harvey." *Journal of Flood Risk Management* 15 (2): e12778. <https://doi.org/10.1111/jfr3.12778>.
- Sarica, G. M., T. Zhu, W. Jian, E. Y. M. Lo, and T. C. Pan. 2021. "Spatio-temporal Dynamics of Flood Exposure in Shenzhen from Present to Future." *Environment and Planning B: Urban Analytics and City Science* 48 (5): 1011–1024. <https://doi.org/10.1177/2399808321991540>.
- Shen, P., L. Zhang, H. Chen, and R. Fan. 2018. "EDDA 2.0: Integrated Simulation of Debris Flow Initiation and Dynamics Considering two Initiation Mechanisms." *Geoscientific Model Development* 11 (7): 2841–2856. <https://doi.org/10.5194/gmd-11-2841-2018>.
- Shi, P., X. Yang, F. Liu, M. Li, H. Pan, W. Yang, J. Fang, et al. 2015. "Mapping Multi-Hazard Risk of the World." In *World Atlas of Natural Disaster Risk*, 287–306.
- Tien Bui, D., Q. P. Nguyen, N. D. Hoang, and H. Klempe. 2017. "A Novel Fuzzy K-Nearest Neighbor Inference Model with Differential Evolution for Spatial Prediction of Rainfall-Induced Shallow Landslides in a Tropical Hilly Area Using GIS." *Landslides* 14 (1): 1–17. <https://doi.org/10.1007/s10346-016-0708-4>.
- Tilloy, A., B. D. Malamud, H. Winter, and A. Joly-Laugel. 2019. "A Review of Quantification Methodologies for Multi-Hazard Interrelationships." *Earth-Science Reviews* 196:102881. <https://doi.org/10.1016/j.earscirev.2019.102881>.
- Van Westen, C. J., T. W. Van Asch, and R. Soeters. 2006. "Landslide Hazard and Risk Zonation—why is it Still so Difficult?" *Bulletin of Engineering Geology and the Environment* 65 (2): 167–184. <https://doi.org/10.1007/s10064-005-0023-0>.
- Wang, J., Z. He, and W. Weng. 2020. "A Review of the Research Into the Relations Between Hazards in Multi-Hazard Risk Analysis." *Natural Hazards* 104 (3): 2003–2026. <https://doi.org/10.1007/s11069-020-04259-3>.
- WMO (World Meteorological Organization). 1969. "Manual for Depth-Area-Duration Analysis of Storm Precipitation." WMO-No. 237. Geneva, Switzerland.
- WMO (World Meteorological Organization). 2009. "Manual for Estimation of Probable Maximum Precipitation." WMO-No. 1045. Geneva, Switzerland.
- Xiao, T., and L. M. Zhang. 2023. "Data-driven Landslide Forecasting: Methods, Data Completeness, and Real-Time Warning." *Engineering Geology* 317:107068. <https://doi.org/10.1016/j.enggeo.2023.107068>.
- Xiao, T., L. M. Zhang, R. W. M. Cheung, and S. Lacasse. 2023. "Predicting Spatio-Temporal man-Made Slope Failures Induced by Rainfall in Hong Kong Using Machine Learning Techniques." *Géotechnique* 73 (9): 749–765. <https://doi.org/10.1680/jgeot.21.00160>.
- Xing, X., C. Wu, J. Li, X. Li, L. Zhang, and R. He. 2021. "Susceptibility Assessment for Rainfall-Induced Landslides Using a Revised Logistic Regression Method." *Natural Hazards* 106 (1): 97–117. <https://doi.org/10.1007/s11069-020-04452-4>.
- Zhang, L. M., L. Gao, S. Y. Zhou, R. W. Cheung, and S. Lacasse. 2017. "Stress Testing Framework for Managing Landslide Risks Under Extreme Storms." In *Advancing Culture of Living with Landslides: Volume 2 Advances in Landslide Science*, edited by M. Mikos, B. Tiwari, Y. Yin, and K. Sassa, 17–32. Cham, Switzerland: Springer. [https://doi.org/10.1007/978-3-319-53498-5\\_3](https://doi.org/10.1007/978-3-319-53498-5_3).
- Zhang, L. L., J. Zhang, L. M. Zhang, and W. H. Tang. 2011. "Stability Analysis of Rainfall-Induced Slope Failure: A Review." *Proceedings of the Institution of Civil Engineers – Geotechnical Engineering* 164 (5): 299–316. <https://doi.org/10.1680/geng.2011.164.5.299>.
- Zhou, S. Y. 2020. "Numerical Simulation of Multi-Hazard Interactions and Stress Testing of Landslide Risks in Hong Kong Under Extreme Storms." Ph.D. Thesis, HKSAR: The Hong Kong University of Science and Technology.
- Zhou, S. Y., L. Gao, and L. M. Zhang. 2019. "Predicting Debris-Flow Clusters Under Extreme Rainstorms: A Case Study on Hong Kong Island." *Bulletin of Engineering Geology and the Environment* 78 (8): 5775–5794. <https://doi.org/10.1007/s10064-019-01504-3>.